Chaotic mixer using electro-osmosis at finite Péclet number

Hideyuki Sugioka*
Frontier Research Center, Canon Inc., 30-2, Shimomaruko 3-chome, Oota-ku, Tokyo 146-8501, Japan
(Received 8 September 2009; revised manuscript received 25 November 2009; published 5 March 2010)

Two pressure-driven streams of two miscible liquids can only mix by diffusion in microfluidic channels because of the low Reynolds number. We present an idea to generate mixing by "chaotic advection" in microscale geometries. That is, we consider using induced-charge electro-osmosis to generate a second flow and then modulate between the pressure-driven and induced-charge flows. By using the combined method consisting of the boundary element method, the Lagrangian particle tracking method, and the random-walk method, we analyze mixing efficiency, mixing time, and mixing length, with the effects of modulation frequency and molecular diffusivity, and compare our proposed mixer with other mixers. By this analysis, we find that chaotic mixing can be produced efficiently in a microfluidic channel by switching between pressure-driven and induced-charge flows in a wide range of Péclet number under the specific condition of Strouhal number. By using our proposed mixer, we can expect to realize efficient chaotic mixing with minimum voltage in an ordinary flow channel with a simple structure without an oblique electric field even at large Péclet number.

DOI: 10.1103/PhysRevE.81.036306 PACS number(s): 47.52.+j, 47.65.−d, 47.63.mf

I. INTRODUCTION

Two pressure-driven streams of two miscible liquids mix only through diffusion in microgeometries. This is because the flows typically have low Reynolds numbers and the residence times are typically too small for efficient molecular diffusion to occur. Hence, efficient mixers are important in the microfluidic applications; e.g., in the homogenization of solutions of regents used in chemical reactions. Because of this importance, several methods for microfluidic mixing have been reported, typically based upon clever geometries [1,2], miniature stirrers [3,4], or external agitations using external fields [5,6].

Recently, mixers that employ a vortex flow around metal posts due to induced-charge electro-osmosis (ICEO) [7–9] are proposed, and they have attracted considerable attention in the context of microfluidic applications [10–19] because they can produce a large vortex flow for mixing and a large net flow for pumping (~mm/s) with a small voltage (~V) by the simple structure. ICEO is different from classical electro-osmosis, because it results from the interaction between the electric field and ions in the electric double layer formed by the polarizing effect of the electric field itself [7–9,20–22]; i.e., the velocity of resulting flow is proportional to the square of the electric field, and thus ICEO can avoid many dc problems such as chemical reactions in an electrolyte.

Aref [23] demonstrated that, when flow patterns form closed orbits, one can induce Lagrangian chaos and effective stirring by alternating periodically between two or more flow patterns. In this context, Zhao and Bau [11] have proposed a chaotic mixer using ICEO in a closed chamber on the basis of Aref's method that uses chaotic advection. In the mixer, periodic switching between a vertical and an oblique electric field is used to produce two kinds of vortex flows around a circular metal cylinder. The chaotic mixer using chaotic advection is important because simple vortex mixers never work in microfluidic channels in the absence of molecular diffusivity (i.e., at infinite Péclet number) because the vortex flow is also a laminar flow.

However, mixing must be produced in a directional microfluidic channel in many realistic applications such as micro total analysis systems and biological diagnostic systems. Further, to satisfy the requirements for miniaturization and low-voltage design, we require an ICEO mixer that can be operated in the absence of an oblique electric field. Apparently, the design concept of an ICEO mixer in a flow channel is different from that of the closed chamber. Thus, a chaotic ICEO mixer operated in a directional flow channel without an oblique electric field is important as the simplest chaotic mixer that works well in a wide range of Péclet number.

Nevertheless, thus far, no attempt has been made for producing chaotic mixing by using a directional flow itself along with a vortex flow. Thus, we consider using induced-charge electro-osmosis to generate a second flow and then modulates between the pressure-driven and induced-charge flows. In this study, we focus on a chaotic ICEO mixer that switches between a pressure-driven directional flow and a vortex flow produced by the application of a vertical electric field and elucidate its design concept by using the boundary element method combined with the thin double layer approximation. Further, because Péclet number is not truly infinite in a real channel, we consider finite Péclet number by using the random-walk method along with Lagrangian particle tracking method. Furthermore, we compare our proposed chaotic ICEO mixer with other several ideas that have been proposed to mix two miscible streams.

This paper is presented in five sections. In Sec. II, we describe theory for a geometry model, a flow model, the Lagrangian particle tracking method with the box counting method, the random-walk method for the analysis of finite molecular diffusivity, and a simple model at infinite Péclet number. Based on these models, the results for the basic performance of chaotic ICEO mixers at infinite Péclet number, the effect of switching period, and the effect of molecular diffusivity, are presented in Sec. III. Following a discussion in Sec. IV, our conclusions are summarized in Sec. V.

*sugioka.hideyuki@canon.co.jp

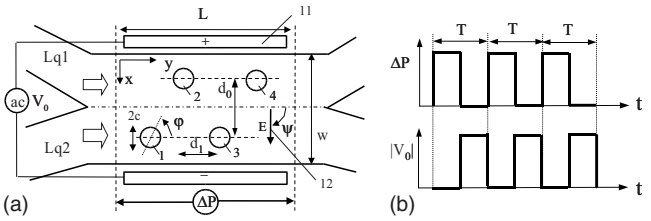

FIG. 1. Schematic diagram of chaotic ICEO mixer. (a) Geometry; (b) switching method. 1–4: metal posts that induce quadruple electro-osmotic flow; 11: pair of electrodes; and 12: electric field. Here, $L=2.25w$ and $w=100$ μm are the length and width of the periodic part of the rectangular channel. Lq1 and Lq2 are two liquids, and $c=0.1w$ is the radius of the metal posts; $x_1=x_3=0.5w+d_0/2$, $x_2=x_4=0.5w-d_0/2$, $y_1=d_1$, $y_2=2d_1$, $y_3=3d_1$, $y_4=4d_1$, $d_0=0.6w$, $d_1=0.45w$, where (x_i,y_i) are the coordinates of the ith number.

II. THEORY

A. Geometry model

Figure 1 shows a schematic diagram of the chaotic ICEO mixer that uses a pressure-driven directional flow and a vortex flow. In Fig. 1(a), we assume that two liquids (Lq1, Lq2) mix in the rectangular channel. As shown in Fig. 1(a), to produce a vortex flow due to ICEO, we typically place four circular metal cylinders of radius $c=0.1w$ at the positions (x_i,y_i) in a rectangular channel of length $L=2.25w$ and width $w=100$ μm, where x_i and y_i are the coordinates of the center of the cylinder of the ith number; e.g., $x_1=x_3=0.5w+d_0/2$, $x_2=x_4=0.5w-d_0/2$, $y_1=d_1$, $y_2=2d_1$, $y_3=3d_1$, $y_4=4d_1$, $d_0=0.6w$, and $d_1=0.45w$. In Fig. 1, the vortex flow produced by the zig-zag structure is characterized by d_0 and d_1. As shown in Fig. 1(b), we alternate between period 1 $(\Delta P\neq 0, V_0=0)$ and period 2 $(\Delta P=0, V_0\neq 0)$ to produce chaotic mixing, where ΔP is a pressure difference between the inlet and outlet, and V_0 is the voltage applied to the electrodes.

B. Flow model

Numerically, we consider a two-dimensional quasistatic Stokes flow without Brownian motion [19,24,25]; i.e., we consider the limit in which the Reynolds number Re tends to zero and the Péclet number is infinite. We assume the posts of the metal cylinder to be polarizable in an electrolytic solution under a dc or ac electric field. The motion of the surrounding fluid must satisfy Stokes equations modified by the inclusion of an electrical stress. However, by using matched asymptotic expansion [26], we can reduce them to the classical Stokes equations as follows:

$$\mu\nabla^2\boldsymbol{v}-\nabla p=0,\quad \nabla\cdot\boldsymbol{v}=0, \tag{1}$$

$$\text{On}\ \ S_{\mathrm{p}}^{+(j)}(\boldsymbol{E}\neq 0):\boldsymbol{v}^{(j)}=\boldsymbol{v}_{\mathrm{s}}^{(j)}, \tag{2}$$

$$\text{On}\ \ S_{\mathrm{p}}^{+(j)}(\boldsymbol{E}=0):\boldsymbol{v}^{(j)}=0 \tag{3}$$

where $S_{\mathrm{p}}^{+(j)}$ denotes the surface defined as the outer edge of the double layer, on the j's metal cylinder $(j=1,2,\ldots,N)$. Further, N is the number of the metal cylinders, $\boldsymbol{E}$ is the electric field, $\boldsymbol{v}$ is the velocity, and p is the pressure. Under a wide range of conditions, the local slip velocity $\boldsymbol{v}_s^{(j)}$ is given by the Helmholtz-Smoluchowski formula,

$$\boldsymbol{v}_s^{(j)}=-\frac{\epsilon\zeta^{(j)}}{\mu}\boldsymbol{E}_{\mathrm{s}}^{(j)} \tag{4}$$

where $\boldsymbol{E}_{\mathrm{s}}^{(j)}$ is the tangential component of the electric field, μ $(\sim 1$ mPa·s) is the viscosity, ϵ $(\sim 80\epsilon_0)$ is the dielectric permittivity of the solvent (typically water), and ϵ_0 is the vacuum permittivity. Here, a zeta potential $\zeta^{(j)}$ around the j's metal is generally defined as $\zeta^{(j)}=\phi_i^{(j)}-\phi_f^{(j)}$, where $\phi_i^{(j)}$ is the electric potential of the metal cylinder that is equal to the electric potential without double layer, and $\phi_f^{(j)}$ is the electric potential just outside the double layer

To consider the slip velocity under a bounded condition, we solve the electric potentials ($\phi_i^{(j)}$ and $\phi_f^{(j)}$) before calculating a flow field by the boundary element method based on the following Laplace's equation, $\nabla^2\phi=0$. On the one hand, we use the Dirichlet boundary condition for the upper and lower walls (electrodes); i.e., $\phi=+0.5V_0$ at $x=0$, $\phi=-0.5V_0$ at $x=w$, where V_0 is an applied voltage across the channel. On the other hand, we use the Neumann boundary condition for the left and right walls; i.e., $\boldsymbol{n}\cdot\nabla\phi=0$ at $y=0$ and L, where $\boldsymbol{n}$ is the surface-normal unit vector. In addition to those boundary conditions, to obtain a final potential, we also use the Neumann boundary condition (i.e., $\boldsymbol{n}\cdot\nabla\phi=0$) on the metal surface. Further, to obtain a initial potential, we use the condition that j's metal cylinder have an unknown surface potential $\phi_i^{(j)}$ and require the electrical neutral condition that $\oint_{(j)}(\boldsymbol{n}\cdot\nabla\phi)ds=0$. Thus, we can numerically calculate a flow field for a bounded domain. It should be noted that we use the boundary condition that the velocity on the wall of the channel is zero and that the pressures of the inlet and outlet are P_1 and P_2, respectively. On the basis of Eqs. (1)–(4), we calculate the flow fields of the ICEO mixer for a bounded domain by the boundary element method. Further, it is convenient to define the representative velocity of a vortex as $\boldsymbol{U}_0(=cE_0^2/\mu)$ [7], where c is the radius of the metal posts and $E_0=|\mathbf{E}|=V_0/w$. Note that to obtain a precise flow field near the wall and the metal surfaces, we use analytical integration to obtain the matrix elements of the boundary element method because the Gauss integration produces a large error near the wall.

C. Lagrangian particle tracking method with box counting method

The Lagrangian particle tracking method in mixing is an analyzing method to visualize a mixing state by tracking passive (tracer) particles in flow velocity fields on the basis of the Lagrangian analysis of motion [4,11]; i.e., $d\mathbf{r}/dt=\boldsymbol{v}(\mathbf{r},t)$. In the simulation, we switch between two flow patterns during a period T; we apply the first flow pattern for $0<t<T/2$ and then the second pattern for $T/2<t<T$. This process is repeated continuously over time, and passive particles are moved and spread. Note that we use periodical condition when we move the particles to consider a long channel with a short channel. By the Lagrangian particle tracking method, we obtain images of the distribution of par-

ticles and visually evaluate the performance of the mixer for various parameters.

To evaluate the mixing performance quantitatively, we use the box counting method [4]; we define the stirring index ε as $\varepsilon_j=\Sigma_{i=1}^{i=K}\omega_{ij}/K$, where $\omega_{ij}=n_{ij}/n_{\mathrm{ave,j}}$ if $n_{ij}<n_{\mathrm{ave,j}}$, and $\omega_{ij}=1$ if $n_{ij}\geq n_{\mathrm{ave,j}}$. Here, $n_{\mathrm{ave,j}}=N_j/K$, N_j is the total number of particle j, K is the number of boxes, and n_{ij} is the number of particle j in the ith box. Note that particle 1 and 2 are corresponding to upper (red) and lower (blue) particles, respectively, and particle 0 is a red or blue particle; i.e., $n_{i0}=n_{i1}+n_{i2}$ and $N_0=N_1+N_2$. Similarly, we can define ε_3 as the stirring index corresponding to $n_{i3}=\sqrt{n_{i1}n_{i2}}$ and $N_3=\sqrt{N_1N_2}$. Through this paper, we use the values that $N_0=20\times40\times2=1600$, $N_1=N_2=20\times40=800$, $N_3=800$, and $K=10\times20=200$. In this case, $n_{\mathrm{ave},0}=8$, $n_{\mathrm{ave},1}=n_{\mathrm{ave},2}=4$, and $n_{\mathrm{ave},3}=4$.

If particles are concentrated in a small region, few overpopulated boxes (boxes under the condition that $n_{ij}>n_{\mathrm{ave,j}}$ and $\omega_{ij}=1$) and many empty boxes (boxes under the condition that $n_{ij}=0$ and $\omega_{ij}=0$) are created. In this case, ε approaches 0. However, if particles are distributed uniformly throughout the channel, many boxes containing the average number of particles (boxes under the condition that $n_{ij}\sim n_{\mathrm{ave,j}}$ and $\omega_{ij}\sim1$) are created. In this case, ε_j approaches 1. Hence, ε_j is interpreted as the stirring index. In particular, ε_3 is useful to evaluate the degree of mixing between particles 1 and 2.

D. Random-walk method for the analysis of finite molecular diffusivity

Random walks are strongly related to diffusive process [27]; i.e., normal diffusion of tracers in liquids is result of the random walks, and that the variance of the ensemble of tracers spreads as

$$\sigma^2(t)=\langle x^2(t)\rangle-\langle x(t)\rangle^2=2Dt, \tag{5}$$

where D is the molecular diffusivity [$x(t)$ represents one dimensional motion]. If the tracer particles take step length l, with a probability distribution function for step lengths

$$P_{\mathrm{rw}}(l)=\frac{1}{\sqrt{2\pi}\sigma}e^{-l^2/2\sigma^2}, \tag{6}$$

the central limit theorem shows that

$$D=\frac{\langle l^2\rangle-\langle l\rangle^2}{2\Delta t}, \tag{7}$$

where $\langle l^n\rangle$ are the moments of P_{rw}, and Δt is the time between each step.

Thus, molecular diffusion is simulated by the random-walk method combined with Lagrange particle tracking method; i.e., at each time step, after moving particles as $\mathbf{r}_{\mathrm{L}}(t)\simeq\mathbf{r}(t-\Delta t)+\mathbf{v}(\mathbf{r},t-\Delta t)\Delta t$, we move tracer particles as $\mathbf{r}(t)=\mathbf{r}_{\mathrm{L}}(t)+\Delta\mathbf{r}_{\mathrm{rw}}$, where $\Delta\mathbf{r}_{\mathrm{rw}}=(\Delta x,\Delta y)$. Here, Δx and Δy are the random numbers that satisfy Eq. (5), and they are generated by the box-muller method. In the algorithm of the random-walk process, if a fluid particle moves into the region of circular cylinders, we do not move the particle.

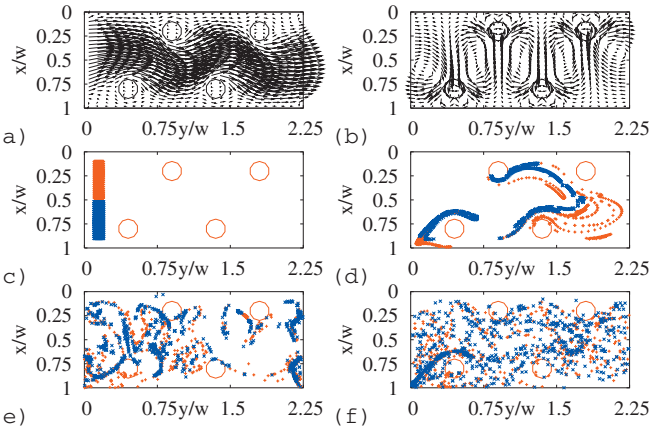

FIG. 2. (Color) Performance of chaotic ICEO mixer that has a zig-zag structure of four metal posts (type A). (a) Flow 1 ($E_0=0$); (b) Flow 2 ($E_0\neq0,\psi=90°$); (c) $t/T_0=0$; (d) $t/T_0=100$; (e) $t/T_0=200$; and (f) $t/T_0=500$. Here, $d_0/w=0.6$ and $d_1/w=0.45$. (a) and (b) Two flow fields; (a) a directional flow resulting from a pressure difference $T_0\Delta P/\mu$ (=2.4) when $\boldsymbol{E}=0$ and (b) a vortex flow resulting from electro-osmosis induced around cylindrical metal posts by the application of an electric field $\boldsymbol{E}=E_0\boldsymbol{i}$ ($T_0U_0/w=T_0cE_0^2/w\mu=0.04$) when $T_0\Delta P/\mu=0$. If $T_0=1$ mm/s, $\mu=1$ mPa·s, and $w=100$ μm, a directional flow and a vortex flow are driven by $\Delta P=2.4$ Pa and $E_0=2.38$ V/m ($U_0=4$ mm/s), respectively. (c)–(f) Distribution of passive tracer particles at $T/2T_0=20$.

E. Simple model at infinite Péclet number

As a first attempt, we can assume that

$$\varepsilon(t)=\varepsilon_{\max}(1-e^{-t/\tau_m}), \tag{8}$$

where $\varepsilon_{\max}$ is a maximum or saturated value and τ_m is a time constant of the mixing phenomenon. If we define a mixing time t_m as the time when $\varepsilon(t)$ reaches $0.95\varepsilon_{\max}$, $t_m/\tau_m=-\ln0.05\sim3$. To modulate between flows, we consider that considerable motions of fluid particles are required such that $U_0T>d_0$ and $U_1T>d_1$; i.e., $1/\mathrm{St}_0\equiv U_0/fd_0>1$ and $1/\mathrm{St}_1\equiv U_1/fd_1>1$, where f is a switching frequency and U_1 is an average velocity of a pressure-driven flow. Here, St_0 and St_1 are Strouhal numbers related to a vortex flow and a pressure-driven flow, respectively. Strouhal number is a dimensionless number oscillating flow mechanisms. Thus, we propose following phenomenological formulations as a first attempt;

$$\varepsilon_{\max}=C_1(1-e^{-1/\mathrm{St}_1})(1-e^{-1/\mathrm{St}_0}), \tag{9}$$

$$t_m/T_0=C_2+C_3e^{-1/\mathrm{St}_0f(T)}+C_4e^{-1/\mathrm{St}_1f(T)}, \tag{10}$$

$$L_m=U_1t_m, \tag{11}$$

where T_0 is a time scale. Here, C_1, C_2, C_3, and C_4 are constant parameters, while $f(T)$ is a function of T.

III. RESULTS

A. Basic performance of chaotic ICEO mixers at infinite Péclet number

Figure 2 shows the performance of the chaotic ICEO mixer that has a zig-zag structure of four metal posts (type

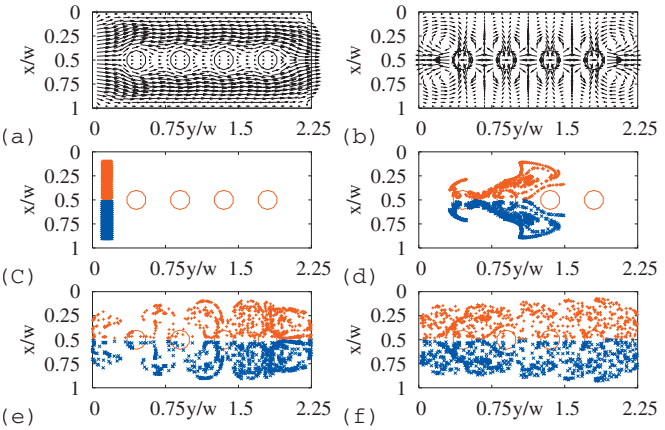

FIG. 3. (Color) Performance of ICEO mixer that has a linear geometry of four metal posts (type B). (a) Flow 1 ($E_0=0$); (b) Flow 2 ($E_0\neq 0, \psi=90°$); (c) $t/T_0=0$; (d) $t/T_0=100$; (e) $t/T_0=200$; and (f) $t/T_0=500$. Here, $d_0/w=0.6$ and $d_1/w=0.45$. (a) and (b): Two flow fields; (a) directional flow resulting from a pressure difference $T_0\Delta P/\mu=2.4$ when $\boldsymbol{E}=0$ and (b) vortex flow resulting from electro-osmosis induced around cylindrical metal posts when $\boldsymbol{E}=E_0\boldsymbol{i}$ $T_0U_0/w=T_0cE_0^2/w\mu=0.04$, and $T_0\Delta P/\mu=0$; Typically, $T_0=1$ mm/s, $\mu=1$ mPa·s, and $w=100$ μm. (c)–(f): Distribution of passive tracer particles at $T/2T_0=20$.

A). Here, $d_0/w=0.6$ and $d_1/w=0.45$. Figures 2(a) and 2(b) show two flow fields: (a) a directional flow resulting from a pressure difference $T_0\Delta P/\mu(=2.4)$ when $\boldsymbol{E}=0$ and (b) a vortex flow resulting from electro-osmosis induced around cylindrical metal posts by the application of an electric field $\boldsymbol{E}=E_0\boldsymbol{i}$ $(T_0U_0/w=T_0cE_0^2/w\mu=0.04)$ when $T_0\Delta P/\mu=0$, where T_0 is a time scale; e.g., if $T_0=1$ mm/s, $\mu=1$ mPa·s,

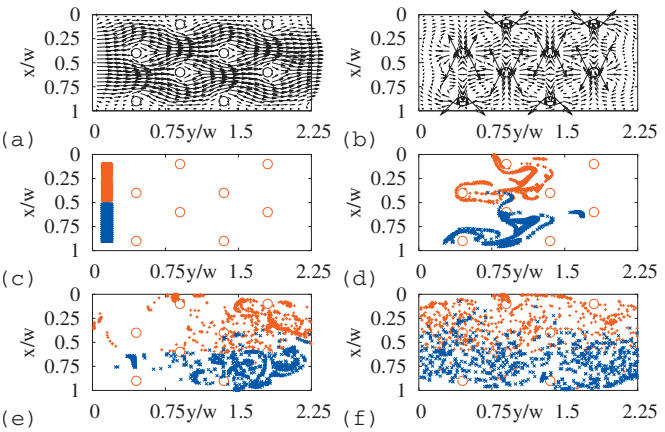

FIG. 4. (Color) Performance of ICEO mixer that has 8 particles (type C). (a) Flow 1 ($E_0=0$); (b) Flow 2 ($E_0\neq 0, \psi=90°$); (c) $t/T_0=0$; (d) $t/T_0=100$; (e) $t/T_0=200$; and (f) $t/T_0=500$. Here, $d_0/w=0.6$ and $d_1/w=0.45$. (a) and (b): Two flow fields; (a) directional flow resulting from a pressure difference $T_0\Delta P/\mu=2.4$ when $\boldsymbol{E}=0$ and (b) vortex flow resulting from electro-osmosis induced around cylindrical metal posts when $\boldsymbol{E}=E_0\boldsymbol{i}$, $T_0U_0/w=T_0cE_0^2/w\mu=0.04$, and $T_0\Delta P/\mu=0$; Typically, $T_0=1$ mm/s, $\mu=1$ mPa·s, and $w=100$ μm. (c)–(f): Distribution of passive tracer particles at $T/2T_0=20$. Here, $x_1/w=x_3/w=0.4$, $x_2/w=x_4/w=0.1$, $x_5/w=x_7/w=0.9$, $x_6/w=x_8/w=0.6$, $y_1/w=x_5/w=0.45$, $y_2/w=x_6/w=0.90$, $x_3/w=x_7/w=1.35$, and $x_4/w=x_8/w=1.80$.

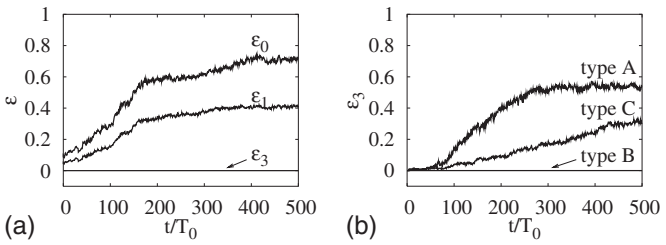

FIG. 5. Dependence of stirring index ε on time. (a) ε vs time for type B; (b) ε vs time for types A to B. Here, $T_0U_0/w=T_0cE_0^2/w\mu=0.04$ and $T_0\Delta P/\mu=2.4$.

and $w=100$ μm, a directional flow and a vortex flow are driven by $\Delta P=2.4$ Pa and $E_0=2.38$ V/m ($U_0=4$ mm/s), respectively. In Fig. 2(a), we observe a typical pressure flow with viscosity; however, it resembles a winding flow of the presence of metal posts near the wall. In Fig. 2(b), we observe large vortices across the channel; they are produced by the presence of a pair of upper and lower metal posts. In Figs. 2(c)–2(f), we show the dispersion of 1600 particles at various times. As shown in Figs. 2(c)–2(f), chaotic mixing is produced by switching between the two flows. Here, the time interval is $T/2T_0=20$. In Fig. 2(c), to examine the mixing between the two liquids emanating from the left of the channel, we place particle 1 (red) and particle 2 (blue) near the inlet; particle 1 (red) region, $0.1\leq x/w<0.5$; particle 2 (blue) region, $0.5<x/w\leq 0.9$. The simulation begins from the interval in which the directional flow is generated. The particles move from the left to the right along the streams of the directional flow shown in Fig. 2(a). After the interval, the particles are subjected to the vortex flow shown in Fig. 2(a). Figure 2(d) shows the distribution of the particles at $t/T_0=100$. Although the particles are subjected to the directional flow three times and the vortex flow two times across the channel, the switching times are not sufficient for mixing. Figure 2(e) shows that mixing at $t/T_0=200$ is also not sufficient for achieving a uniform distribution of particles. Figure 2(e) shows that at $t/T_0=500$, the particle 1 (red) and particle 2 (blue) spread over the entire mixing domain. An efficient mixer should be capable of producing such a result. Note that we consider a periodic boundary condition in order to represent a long channel as a short channel.

Figure 3 shows the performance of the ICEO mixer that has a linear geometry of four metal posts (type B). As shown in Fig. 3, both particles do not mix each other, although upper (red) and lower (blue) particles are dispersed independently in upper and lower regions, respectively. Namely, a symmetrical structure in which the plane of symmetry is at $x=w/2$ has a drawback in that it divides the flow into two symmetrical regions; i.e., the upper and lower regions. Figure 4 shows the performance of ICEO mixer that has eight particles (type C). As shown in Fig. 4, it is disadvantageous to place many small metal posts across the channel, because they create small vortices separated from each other and do not contribute to large-scale mixing. Thus, we believe that the zig-zag structure of type A is more suitable for chaotic mixing in the flow channel than the linear structure of type B and the 8 particle structures of type C.

Next, we present a quantitative evaluation of the mixing problem. Here, we use ε_3 to evaluate mixing efficiency since

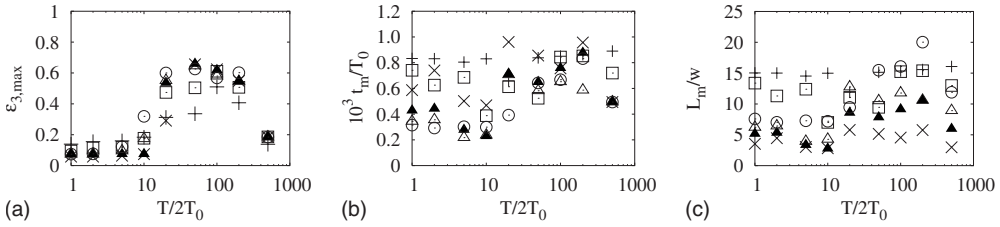

FIG. 6. Dependence of ε_3, t_m, and L_m on $T/2$ at infinite Péclet number for type A. Symbols show numerical results; i.e., plus, open square, and open triangle show the numerical results at $T_0U_0/w=0.01$, 0.02, and 0.04, respectively, when $T_0\Delta P/\mu=1.8$, while cross, closed triangle, and open circle show the numerical results at $T_0\Delta P/\mu=0.6$, 1.2, and 2.4, respectively, when $T_0U_0/w=0.04$.

ε_0 and ε_1 can increase even when particle 1 (red) and particle 2 (blue) are stirred independently in type B, as shown in Fig. 5(a). Figure 5(b) shows the dependence of ε_3 on time for various ICEO mixers (types A–C). As shown in Fig. 5(b), type A shows good mixing performance, while mixing performance of type B is zero. Furthermore, although it is difficult to determine the mixing time t_{mix} from Fig. 2 of the trajectory method, we can obtain $t_{\mathrm{mix}}\simeq 350$ ms for type A from Fig. 5(b) by the box counting method.

B. Effect of switching period

Next, we show the effect of the switching period. Figure 6 shows the dependence of ε_3, t_m, and L_m on $T/2$ at infinite Péclet number for type A. As shown in Fig. 6, there exists an appropriate switching period for producing chaotic mixing, and the values of ε_3 are small when the switching periods are too short or long to mix the liquids. However, as mentioned before, those results should be replotted on $\mathrm{St}_0(=fd_0/U_0)$ and $\mathrm{St}_1(=fd_1/U_1)$ as shown in Fig. 7. Here, d_0 (=0.6w) and d_1 (=0.45w) are characteristic lengths of vortex and directional flows. As shown in Fig. 7, we observe that the analytical results of ε_3, t_m, and L_m agree fairly well with the numerical results, although the agreement between numerical results and analytical results of t_m and L_m is very bad in Figs. 7(b) and 7(c). Here, we set that $C_1=0.62$, $C_2=300$, $C_3=400$, $C_4=600$, and $f(T)=0.3(T/20)^{1.5}$ in Eqs. (9)–(11). From Figs. 7(a) and 7(d), we find that mixing efficiency is enhanced for the suitable Strouhal number ($\mathrm{St}_0<1$ and $\mathrm{St}_1<1$). Further, from Figs. 7(b), 7(c), 7(e), and 7(f), mixing time and length are approximately 1 s and 1 mm, respectively, in the suitable range of Strouhal number ($\mathrm{St}_0<1$ and $\mathrm{St}_1<1$).

Figures 8(a)–8(c) [Figs. 8(d)–8(f)] show the dependence of ε_3, t_m, and L_m, respectively, on $U_0(U_1)$ at infinite Péclet number for type A. In Fig. 8, lines show the analytical results of the simple model, and symbols show numerical results. As shown in Fig. 8, we observe that the analytical results of ε_3, t_m and L_m also agree fairly well with the numerical results. Further, from Figs. 8(a) and 8(d), we find that mixing is enhanced when $1/\mathrm{St}_0>1$ and $1/\mathrm{St}_1>1$ as predicted by the simple model. Furthermore, in Figs. 8(b), 8(c), 8(e), and 8(f), we also find that mixing time and length are approximately 1 s and 1 mm, respectively, in the suitable range of Strouhal number ($\mathrm{St}_0<1$ and $\mathrm{St}_1<1$).

C. Effect of molecular diffusivity

Next, we show the effect of molecular diffusivity. Figure 9 shows the dependence of ε_3, t_m, and L_m on f in the pres-

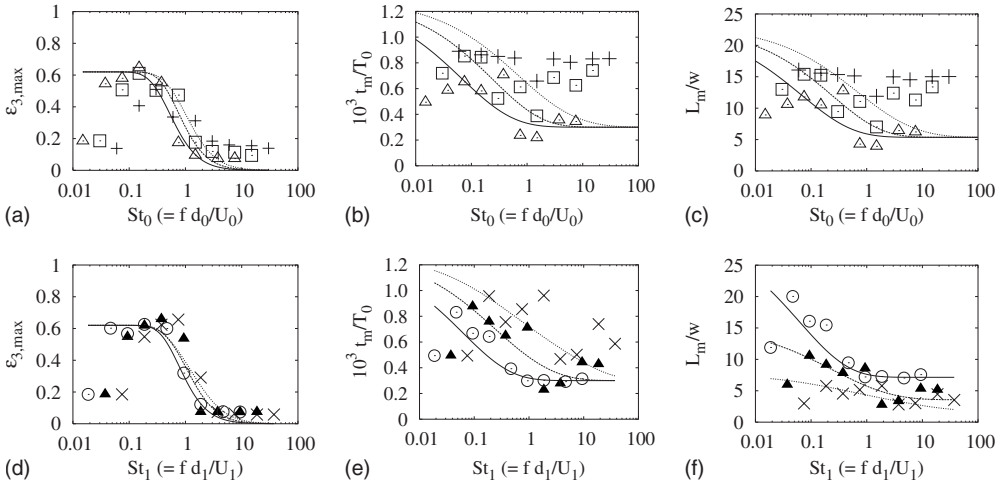

FIG. 7. Dependence of ε_3, t_m, and L_m on f at infinite Péclet number. In (a) to (c), $T_0\Delta P/\mu=2.4$; in (d) to (f), $T_0U_0/w=0.04$. Here, the results of Fig. 6 are replotted on (a)–(c) St_0 and St_1 (d)–(f). Dotted, broken, and solid lines show the analytical results by using Eqs. (9)–(11) at $T_0U_0/w=0.01$, 0.02, and 0.04 [at $T_0\Delta P/\mu=0.63$, 1.2, and 2.4], respectively, in (a)–(c) [in (d)–(f)]. Symbols show numerical results; i.e., plus, open square, and open triangle show the numerical results at $T_0U_0/w=0.01$, 0.02, and 0.04, respectively, when $T_0\Delta P/\mu=1.8$, while cross, closed triangle, and open circle show the numerical results at $T_0\Delta P/\mu=0.6$, 1.2, and 2.4, respectively, when $T_0U_0/w=0.04$.

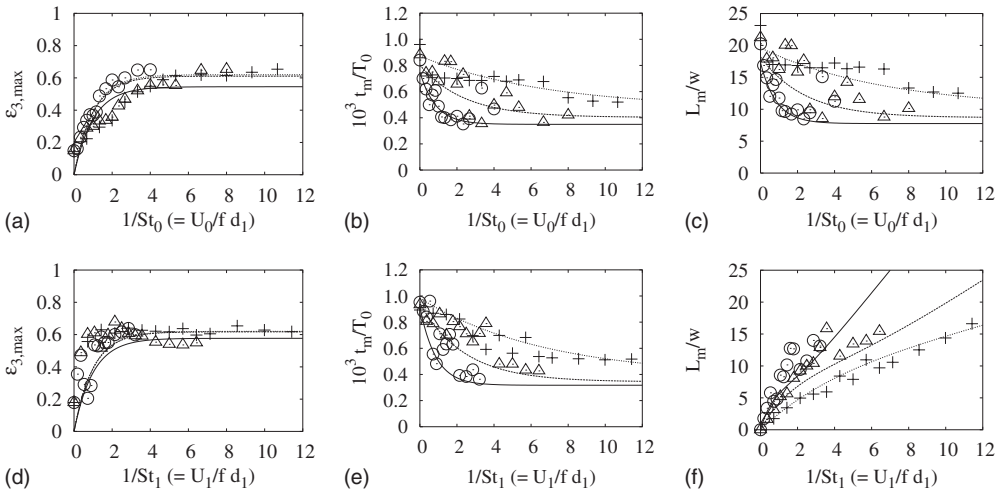

FIG. 8. Dependence of ε_3, t_m, and L_m on U_0 and U_1 at infinite Péclet number ($D=0\ \mathrm{m}^2/\mathrm{s}$) for type A. In (a) to (c), $T_0\Delta P/\mu=2.4$; in (d) to (f), $T_0U_0/w=0.04$. Lines show the analytical results of the simple model; i.e., solid, dashed, and dotted lines show the analytical results of $T/2T_0=20$, 40, and 80, respectively. Symbols show numerical results; i.e., solid, dashed, and dotted lines plus, open triangle, and open circle show the numerical results of $T/2T_0=20$, 40, and 80, respectively.

ence of molecular diffusivity ($D=1.0^{-9}\ \mathrm{m}^2/\mathrm{s}$) for type A. Because of the presence of molecular diffusivity, mixing efficiency is not so low even in the unsuitable range of Strouhal number ($\mathrm{St}_0>1$ and $\mathrm{St}_1>1$) as shown in Figs. 9(a) and 9(d). Nevertheless, we can see the enhancement of mixing efficiency in the suitable range of Strouhal number ($\mathrm{St}_0<1$ and $\mathrm{St}_1<1$). Further, for typical values, mixing time and length are approximately 400 to 800 ms and 0.5 to 1.5 mm, respectively, in the suitable range of Strouhal number.

Figure 10 shows the dependence of ε_3, t_m, and L_m on D [Figs. 10(a)–10(c)] and Pe_1 ($=U_1w/D$) [Figs. 10(d)–10(f)] for type A and the simple rectangular mixer (type D) that uses just molecular diffusion, where Pe_1 is a Péclet number for a directional flow. Note that Péclet number is a dimensionless number the rate of advection of a flow to its rate of diffusion. Here, $T_0\Delta P/\mu=2.4$ and $T_0U_0/w=0.04$; $T_0U_1/w=0.024$ and 0.09 for types A and D, respectively. In Figs. 10(d)–10(f), solid and broken lines show the scaling functions that are made to fit numerical results for type D and A, respectively; i.e., for type D, $\epsilon_{\max}=0.85$, $t_m=0.1w\ \mathrm{Pe}_1/U_1$, and $L_m=0.1w\ \mathrm{Pe}$; and for type A, $\varepsilon_{\max}=1.96-\mathrm{Pe}_1^{0.033}$, $t_m/T_0=340[1-e^{-\mathrm{Pe}_1/60}]$, and $L_m/T_0U_1=340[1-e^{-\mathrm{Pe}_1/60}]$. Namely, the mixing time and mixing length of type A are almost constant, while those of type D are proportional to Péclet number. Further, as shown in Figs. 10(e) and 10(f), mixing time and length of type A are shorter than those of type D in the ranges that $\mathrm{Pe}_1>300$ and $\mathrm{Pe}_1>100$, respectively.

Figure 11 shows the performance of simple vortex mixers without switching for the structures of types A–C. Here, $T_0\Delta P/\mu=2.4$ and $T_0U_0/w=0.04$; typically, $T_0=1$ ms, $\mu=1$ mPa·s, and $w=100$ μm. From Fig. 11, we can find that the structure of type A is more effective for mixing than

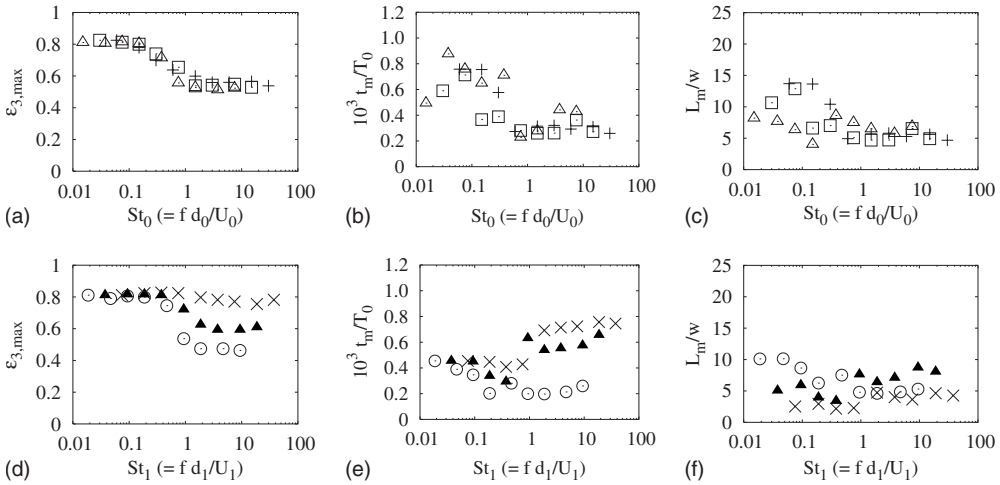

FIG. 9. Dependence of ε_3, t_m, and L_m on f at finite Péclet number ($D=1.0^{-9}\ \mathrm{m}^2/\mathrm{s}$) for type A. In (a) to (c), $T_0\Delta P/\mu=1.8$; in (d) to (f), $T_0U_0/w=0.04$. Symbols show numerical results; i.e., plus, open square, and open triangle show the numerical results at $T_0U_0/w=0.01$, 0.02, and 0.04, respectively, when $T_0\Delta P/\mu=1.8$, while cross, closed circle, and open circle show the numerical results at $T_0\Delta P/\mu=0.6$, 1.2, and 2.4, respectively, when $T_0U_0/w=0.04$.

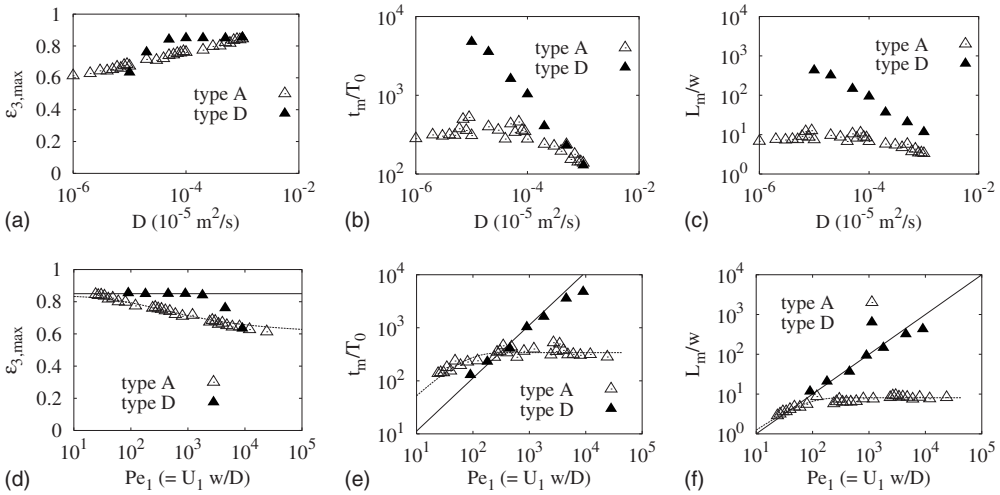

FIG. 10. Dependence of ε_3, t_m, and L_m on D (a) and (c) and Pe_1 ($=U_1w/D$) (d) and (f) for type A and type D. Here, $T_0\Delta P/\mu=2.4$, $T_0U_0/w=0.04$, $T_0U_1/w=0.024$ for type A, and $T_0U_1/w=0.090$ for type D. In (c)–(f), solid and broken lines show the scaling functions that are made to fit numerical results for type D and type A, respectively; for type D, $\epsilon_{\max}=1.96-\mathrm{Pe}_1^{0.022}$, $t_m=0.1w\ \mathrm{Pe}_1/U_1$, and $L_m=0.1w\ \mathrm{Pe}_1$; for type A $\epsilon_{\max}=1.96-\mathrm{Pe}_1^{0.033}$, $t_m/T_0=340[1-e^{-\mathrm{Pe}_1/60}]$, and $L_m/U_1T_0=340[1-e^{-\mathrm{Pe}_1/60}]$; typically, $T_0=1$ ms, $\mu=1$ mPa·s, and $w=100$ μm.

those of type B and type C; i.e., the large vortex flow to across two miscible liquid regions is required for simple vortex mixers to obtain good performance. Further, as shown in Fig. 11(c), mixing times of simple vortex mixers are approximately proportional to logarithm of Pe_0, where Pe_0 ($=U_0w/D$) is a Péclet number for a vortex flow. Furthermore, in Figs. 11(a) and 11(b), the performance of type D is also plotted for the comparison. By this comparison, we can find that the values of t_m of simple vortex mixers are smaller than those of type D in the range that $D<2\times10^{-9}$ m^2/s, and thus it is useful to use vortex flow in this range.

IV. DISCUSSION

At infinite Péclet number and low Reynolds number, we need to use a chaotic mixer proposed by Aref [23], and need to switch fluid orbitals finely. Nevertheless, so far, researchers have only explored the chaotic mixer using two kinds of vortex flows [11]. Thus, we have first shown that the chaotic mixer using a directional flow and a vortex flow is also useful for mixing, although Aref demonstrated that one can generate Lagrangian chaos by alternating between two (or more) different closed-orbit patterns. In particular, the chaotic mixer using a pressure-driven flow and a vortex flow due to ICEO is useful because of its simplicity and effectiveness of applying voltage. Further, different from ordinary chaotic mixers, the proposed chaotic mixer requires the specific modulation frequency to modulate fluid orbitals each other; i.e., by the analysis using the boundary element method combined with the thin double layer approximation, we have first shown that chaotic mixing is produced under the condition that $\mathrm{St}_0=fd_0/U_0<1$ and $\mathrm{St}_1=fd_1/U_1<1$.

A simple microfluidic mixer and simple vortex mixers are also expected to work at finite Péclet number, although these mixers never work at infinite Péclet number and low Reynolds number. To clarify this problem, we have considered finite Péclet number by using random-walk method along with Lagrangian tracking method, and compared our proposed mixer with a simple microfluidic mixer, simple vortex mixers, and other chaotic mixers. From the view point of the random-walk theory, the mixing time of a simple mixer (type D) is estimated by the relation that $\sqrt{2Dt_m^{\mathrm{simple}}}\simeq w/2$; i.e., $t_m^{\mathrm{simple}}\simeq w^2/8D\simeq \mathrm{Pe}_1\ w/8U_1\sim 0.1\mathrm{Pe}_1\ w/U_1$ and $L_m^{\mathrm{simple}}\simeq \mathrm{Pe}_1\ w/8\sim 0.1\mathrm{Pe}_1\ w$. Thus, the numerical results of a simple mixer using the random-walk method along with the Lagrangian particle tracking method are justified. Further, the values that $D=10^{-10}$ m^2/s, $w=100$ μm, and $U_1=1$ to 10 mm/s are the typical values of many BioMEMS applications. For this system, $\mathrm{Pe}_1=U_1w/D=1000$ to 10 000 and $\mathrm{Re}=U_1w/\nu=0.1$ to 1, where ν is the kinematic viscosity of the fluid; the mixing length and mixing time of a simple mixer

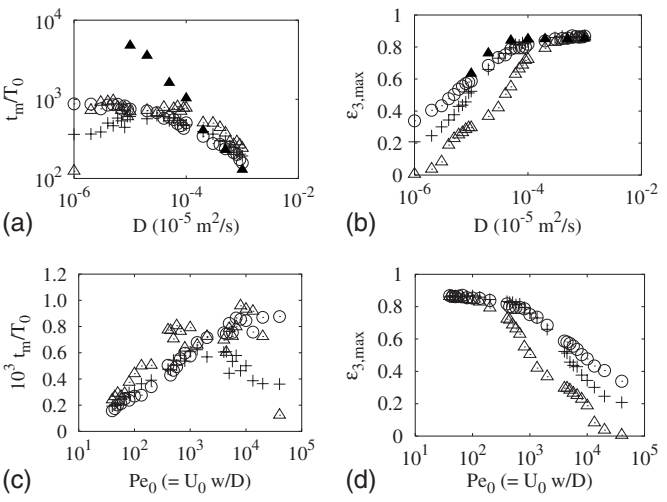

FIG. 11. Performance of simple vortex mixers without switching. Open circle, plus, and open triangle show the numerical results of the simple vortex mixers for the structures of type A, B, and C, respectively. In (a) and (b), the performance of type D (close triangle) is also plotted for the comparison. Here, $T_0\Delta P/\mu=2.4$ and $T_0U_0/w=0.04$; typically, $T_0=1$ ms, $\mu=1$ mPa·s, and $w=100$ μm.

are $t_m^{\text{simple}} \sim 0.1\text{Pe}_1\, w/U_1 = 10$ to 100 s and $L_m^{\text{simple}} \sim 0.1\text{Pe}_1\, w = 1$ to 10 cm, respectively, while the mixing length and mixing time of a chaotic mixer are $t_m^{\text{chaos}} \sim 0.4$ s and $L_m^{\text{chaos}} \sim 1$ mm, respectively. Thus, the proposed chaotic mixer is more effective than the simple microfluidic mixer for many BioMEMS applications. Furthermore, the mixing time of a simple vortex mixer of the structure of type A is $t_m^{\text{vortex}} \sim 0.7$ s at $\text{Pe}_0 = 1000$, and is proportional to $\ln \text{Pe}_0$. Thus, the simple vortex mixer is also more effective than the simple microfluidic mixer. Note that we can see similar discussions in [1]. However, mixing efficiency is decreasing as the Péclet number is increasing in the range that $\text{Pe}_0 > 1000$. Therefore, the chaotic mixer is more effective than simple vortex mixers, since it works well in the wide rage of Péclet number.

To prevent sample dilution, the Harnett *et al.* [10] developed an ICEO mixer using many large triangular posts that form two directional channels for loading and many connecting channels for mixing. Although the ICEO mixer in [10] makes long vortex flows in the x direction and pressure flows in the *y* direction, it is intrinsically a simple vortex mixer because the directional flows are just used to prepare samples without mixing and the vortex flows does not cross the directional flows. Thus, the design concept is completely different from ours. Further, the performance of many passive mixers [1] that use baffles or obstacles that create a tortuous pathway are probably similar to that of a simple vortex mixer because the tortuous pathway also promotes mixing by stretching the interface between the liquids and decreasing the distance over which diffusion must take place. Note that Giona *et al.* [28] showed that mixing is enhanced due to the increase of the intermaterial contact area by the time-periodic sine flow by using the advection-diffusion equation. Furthermore, Glasgow and Aubry [29] analyzed the effect of pulsing the classical electro-osmotic flow rate in one inlet only as well as in the two inlets, and demonstrated that the best results occur when both inlets are pulsed out of phase. In this case, interface is shown to stretch, retain one fold, and sweep through the confluence zone, leading good mixing. Although there are many similar points such that the mixer requires $\text{St}_1 \sim 1$ [30], it is not a chaotic mixer using chaotic advection and the performance is probably similar to that of a simple vortex mixer.

V. CONCLUSION

In conclusion, we have proposed chaotic ICEO mixers that switch a pressure-driven directional flow and a vortex flow and numerically examined their performance. By the boundary element method combined with the thin double layer approximation and the Lagrangian particle method along with random-walk method, we find that (1) chaotic mixing can be efficiently produced by switching between a pressure-driven directional flow and a large vortex flow under the condition that $\text{St}_0 (= f d_0 / U_0) < 1$ and $\text{St}_1 (= f d_1 / U_1) < 1$; (2) the mixing performance of the chaotic mixer that has a large vortex flow due to the zig-zag structure of four metal posts across a channel is better than that of chaotic mixers that have many smaller vortex flows; (3) the mixing time of the proposed chaotic mixer is almost constant in all the range of Péclet number, while the mixing times of a simple microfluidic mixer and a simple vortex mixer are approximately proportional to the Péclet number and the logarithm of the Péclet number, respectively. When Péclet number is relatively large, our proposed method can be useful to produce chaotic mixing at a low voltage in an ordinary microfluidic channel using simple electrodes.

ACKNOWLEDGMENTS

I am grateful to E. Darve for the helpful discussions about the mathematical details of the calculation.

[1] A. D. Stroock, S. K. W. Dertinger, A. Ajdari, I. Mezić, H. A. Stone, and G. M. Whitesides, Science **295**, 647 (2002).
[2] H. Chen and J. Meiners, Appl. Phys. Lett. **84**, 2193 (2004).
[3] J. B. Zhang, G. W. He, and F. Liu, Phys. Rev. E **73**, 056305 (2006).
[4] H. Kim and A. Beskok, J. Micromech. Microeng. **17**, 2197 (2007).
[5] D. A. Boy and B. D. Storey, Phys. Rev. E **76**, 026304 (2007).
[6] B. Stoeber, D. Liepmann, and S. J. Muller, Phys. Rev. E **75**, 066314 (2007).
[7] M. Z. T. Bazant and T. M. Squires, Phys. Rev. Lett. **92**, 066101 (2004).
[8] T. M. Squires and M. Z. T. Bazant, J. Fluid Mech. **509**, 217 (2004).
[9] T. M. Squires and M. Z. T. Bazant, J. Fluid Mech. **560**, 65 (2006).
[10] C. Harnett, J. Templeton, K. Dunphy-Gazman, Y. Senousy, and M. Kanouff, Lab Chip **8**, 565 (2008).
[11] H. Zhao and H. H. Bau, Phys. Rev. E **75**, 066217 (2007).
[12] J. Urbanski, T. Thorsen, J. Levian, and M. Bazant, Appl. Phys. Lett. **89**, 143508 (2006).
[13] D. Burch and M. Z. Bazant, Phys. Rev. E **77**, 055303(R) (2008).
[14] S. Gangwal, O. J. Cayre, M. Z. Bazant, and O. D. Velev, Phys. Rev. Lett. **100**, 058302 (2008).
[15] A. Ramos, A. Gonzalez, A. Castellanos, N. G. Green, and H. Morgan, Phys. Rev. E **67**, 056302 (2003).
[16] A. Ajdari, Phys. Rev. E **61**, R45 (2000).
[17] L. H. Olesen, H. Bruus, and A. Ajdari, Phys. Rev. E **73**, 056313 (2006).
[18] H. Sugioka, Phys. Rev. E **78**, 057301 (2008).
[19] H. Sugioka, Phys. Rev. E **80**, 016315 (2009).
[20] M. Z. Bazant, K. Thornton, and A. Ajdari, Phys. Rev. E **70**, 021506 (2004).
[21] K. T. Chu and M. Z. Bazant, Phys. Rev. E **74**, 011501 (2006).
[22] B. D. Storey, L. R. Edwards, M. S. Kilic, and M. Z. Bazant, Phys. Rev. E **77**, 036317 (2008).
[23] H. Aref, J. Fluid Mech. **143**, 1 (1984).
[24] H. J. Keh, K. D. Horig, and J. Kuo, J. Fluid Mech. **231**, 211 (1991).

[25] H. Zhao and H. Bau, Langmuir **23**, 4053 (2007).
[26] M. C. Fair and J. L. Anderson, J. Colloid Interface Sci. **127**, 388 (1989).
[27] E. R. Weeks and H. L. Swinney, Phys. Rev. E **57**, 4915 (1998).
[28] M. Giona, S. Cerbelli, and A. Adrover, Phys. Rev. Lett. **88**, 024501 (2001).
[29] I. Glasgow and N. Aubry, Lab Chip **3**, 114 (2003).
[30] I. Glasgow, J. Batton, and N. Aubry, Lab Chip **4**, 558 (2004).